Graphical Abstract

Flow correlations and transport behaviour of turbulent slurries in partially filled pipes

Christopher J. Cunliffe, Jonathan M. Dodds, David J. C. Dennis

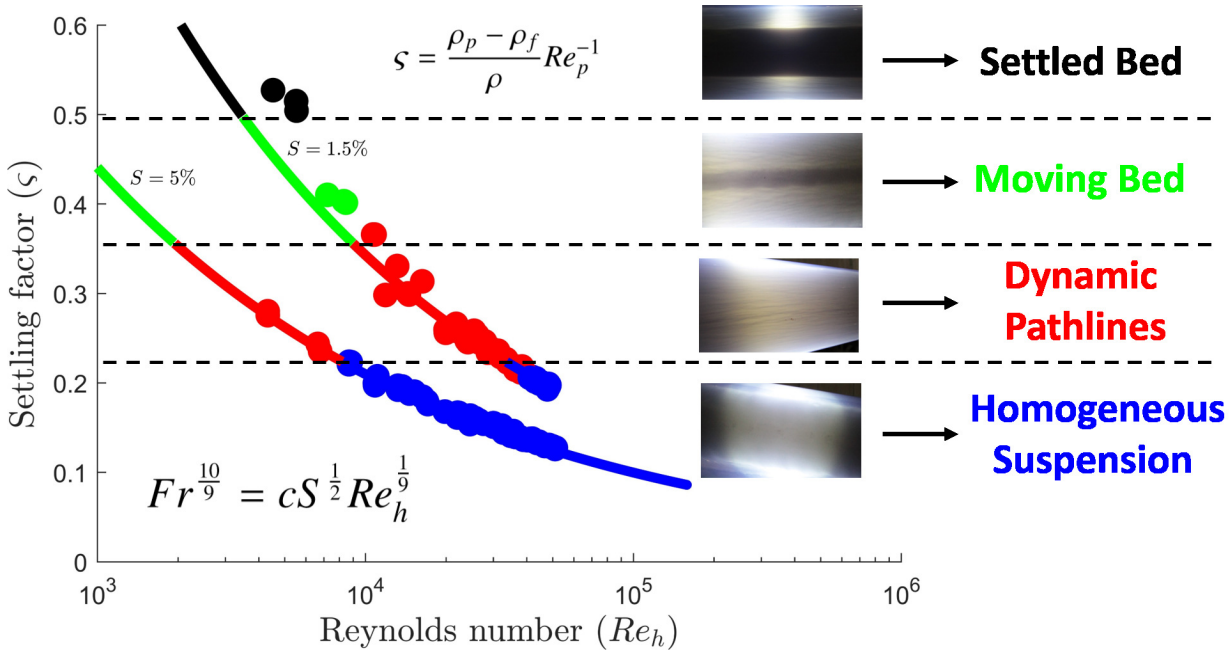

Highlights

Flow correlations and transport behaviour of turbulent slurries in partially filled pipes

Christopher J. Cunliffe, Jonathan M. Dodds, David J. C. Dennis

- Slurry (multiphase and non-Newtonian) flow in partially filled pipes is investigated
- Bulk flow behaviour is accurately predicted using a novel non-dimensional correlation
- Sedimentation behaviour is characterised by a single dimensionless parameter
- A powerful framework for the design of pipe operations is presented
- All findings supported by extensive new experimental database

Flow correlations and transport behaviour of turbulent slurries in partially filled pipes

Christopher J. Cunliffe[a,b], Jonathan M. Dodds[a], David J. C. Dennis[b,*]

[a]*National Nuclear Laboratory, Workington, CA14 3YQ, United Kingdom*
[b]*School of Engineering, University of Liverpool, L69 3GH, United Kingdom*

Abstract

Transportation of fluids in partially filled pipes is common to many areas of industry (e.g. sewerage, mining, and nuclear), yet many aspects remain under-developed, particularly for multiphase and non-Newtonian flows. In this paper a simple framework to enable the accurate prediction of the bulk flow behaviour and settling characteristics of slurries in open conduits is developed and validated experimentally. The experiments involve measurements of flow rate, flow depth and the settling regime for two different solids concentrations of two types of non-colloidal suspensions across a broad range of channel slopes, Reynolds numbers, and Froude numbers. A method is presented that can be used to make a-priori predictions of critical sedimentation velocities, which can inform future pipeline designs and operations to minimise the environmental and commercial costs of slurry transfers, including reducing the risk of pipe blockages. Only one parameter required for this technique is not related to the measurable physical properties of the pipeline or fluid. However, it is empirically shown to be well represented by a single, dimensionless constant for all fluids and pipelines tested.

Keywords: slurry, turbulent, partially filled pipes, non-colloidal suspensions, open channel flow, sedimentation

Nomenclature

α	Pipe incline angle	°	
$\dot{\gamma}_c$	Characteristic shear rate	s^{-1}	
$\dot{m}$	Mass flow rate	kg/m^3	
μ	Dynamic viscosity	Pa s	
ν	Kinematic viscosity	m^2/s	
ν_f	Kinematic viscosity of water	m^2/s	
ρ	Density	kg/m^3	
ρ_f	Density of water	kg/m^3	
ρ_p	Density of solid particle	kg/m^3	
τ_w	Wall shear stress	Pa	
θ	Pipe fill angle	rad	
ς	Settling factor	-	
A	Flow cross-sectional area	m^2	
B	Free surface length	m	
c	Flow constant	-	
D	Pipe diameter	m	
d	Flow depth (verticle bisector)	m	
D_h	Hydraulic diameter	m	
d_p	Particle size diameter	m	
f_d	Darcy friction factor	-	
Fr	Froude number	-	
g	Acceleration due to gravity	m/s^2	
h_f	Frictional head loss	m	
K	Flow consistency index	mPa s^{n_p}	
L	Pipe length	m	
n	Manning's roughness coefficient	$s/m^{1/3}$	
n_p	Flow behaviour index	-	

*Corresponding author
Email address: djcd@liverpool.ac.uk (David J. C. Dennis)

R	Pipe radius	m
R_h	Hydraulic radius	m
Re_h	Hydraulic Reynolds number	-
S	Channel slope	-
T	Temperature	°C
U_b	Bulk velocity	m/s

1. Introduction

Partially filled pipe flows, often gravity-driven, are present in a range of industrial applications and are often used to transport fluids with sediments or particulates, for example sewage and waste-water, as well as slurries in nuclear or mining operations. The partially filled pipe geometry contains features of a full pipe and an open channel flow. However, in comparison to these flows the scientific literature remains underdeveloped for partially filled pipe flow with work often restricted to studies of water. When transporting fluids that contain solid particles, such as in slurry transport applications, there are two additional important considerations. Firstly, there is the question of how well the fluids (now two-phase and non-Newtonian) follow the traditional flow correlations that were derived for water flows and include empirical constants obtained from water flow experiments. And secondly, the settling behaviour of the suspended particles (and its dependence of flow conditions) is critically important in order to avoid deposition and potential blockages, which are potentially extremely disruptive and costly in applications that involve the transport of nuclear waste.

1.1. Partially-filled pipes

The Manning equation predicts the average velocity for gravity driven fluids in open channel flows, with a single empirical parameter (n, termed the Manning coefficient) used to equate the relationship of bulk velocity with the hydraulic radius and channel slope; and hence is one of the most widely cited equations on open channel flow (Powell, 1960). It is a very practical and useful equation for fluid flows possessing a free surface and driven by gravity. In metric units, the Manning equation is written as shown in equation 1 (Manning et al., 1890)

$$V_{Manning} = \frac{1}{n} R_h^{\frac{2}{3}} \sqrt{S}. \quad (1)$$

The empirical coefficient, n, is often called a "roughness coefficient", despite having units of $time/length^{\frac{1}{3}}$, because the value is said to be dependent on the channel wall characteristics. Much work has been done both using and developing the Manning equation over the years. It is widely used as the simple relationship does a remarkably good job in certain situations (particularly if water is the working fluid). However, it has also been developed extensively (often into more complex forms) by researchers who have identified its deficiencies in other scenarios. The nature of the Manning equation means a degree of iteration is required to ascertain the implicit flow depth (Saatci, 1990). Barr et al. (1986) and Akgiray (2005) developed explicit methods for the determination d/D (where d is the flow depth, and D is the pipe diameter). It is common for a constant n based on channel material to be used in practice, especially for a natural channel with varying degrees of sedimentation, and a range of these values are well documented for varying flow scenarios (Chow, 1959; Arcement and Schneider, 1989; Mays, 1999; Phillips and Tadayon, 2006).

Attari and Hosseini (2019) investigated a calibration procedure for the determination of n for a riverbed with varying roughness in the streamwise axis (constant n in the depth axis), based on at least one inflow and the corresponding outflow hydrograph. However, other studies have investigated the variability of n with d in various channels. Camp (1946) showed the variation of n with flow depth graphically using data from Wilcox (1924). Zaghloul (1998) and Akgiray (2004) fitted an expression to this data with various high order polynomials. Zaghloul (1998) then applied this relationship to simulate runoff transport phenomenon, updating existing models to include the effect of varying roughness. Enfinger and Schutzbach (2005), using a scatter graph and various regressive methods, assessed how the value of how the Manning coefficient varies with flow depth for circular channels, to provide a more accurate determination of sewer capacity.

It should be noted that calibration of many roughness models relies on historical empirical data. Various scaling terms have been used to find a value for n in terms of gravitation acceleration (g) and a length scale that is representative of the pipe roughness (Chow, 1959); these were derived theoretically by Gioia and Bombardelli (2001). Yen (1992) recommended a slight modification to dimensionally homogenise the Manning equation, this involved a new roughness coefficient having units of $length^{\frac{1}{6}}$. This was done to correct for the fact that no dependency on *time* is expected if n is purely a representation of pipe roughness, and was achieved by the simple introduction of a term representing g. Other studies have sought to replace n altogether with something

more meaningful. Pomeroy (1983) modified the equation by replacing n and the hydraulic radius (R_h) with a flow rate (Q) and a new coefficient for pipe roughness/smoothness which was invariant with flow depth; this gave a better representation of the flow velocity at various fill levels. Christensen (1984) expanded on this work to replace n with a new constant containing the physically meaningful variables of g, and the equivalent roughness length scale, improving the dimensional meaningfulness of all the parameters in the equation. Yu and Lim (2003) modified the equation to include a more direct measurement of flow resistance for alluvial channels with sand-beds, based on known resistance laws. One drawback to the Manning equation is that is does not contain any parameters representative of the particulate or carrier phase in multiphase flow scenarios. Other studies undertaken in the partially filled turbulent regime using Newtonian, single-phase fluids (generally water) include Nezu and Rodi (1986), Yoon et al. (2012) and Ng et al. (2018).

1.2. Slurry transport

Existing work on the transport of slurries has focused heavily on full-bore pipes and the use of empirical equations to identify a critical velocity, with the implied intention of operating the pipeline near this velocity at a minimum economic cost. It is generally stated in the literature that there is a discrete transition between two flow regimes, the first where partial slurry particles are stationary on the pipe wall, and a second where all slurry particles are moving without any deposition. The velocity at this boundary is defined as the critical velocity (Durand, 1953; Wasp et al., 1977; Swamee, 1995; Kökpınar and Göğüş, 2001).

Work, especially in the nuclear industry, has focused more on the safety aspect of slurry transport, this is due to the high toxicity and novel nature of the waste required for transportation. Poloski et al. (2010) investigated a flow correlation for the identification of critical velocity in a full bore pipe for a slurry with small but dense particles, which is typical for nuclear wastes. Research by Adamson (2011) at Savannah River National Laboratory (SRNL) supported Hanford WTP operations by evaluating the effectiveness of mixing and transferring simulated tank waste. Results showed that water always transfers fewer particles and is a conservative carrier fluid compared to fluids of higher viscosity and yield stresses. Furthermore, dimensional analysis on the yield stress term gave a gravity yield parameter which defined four regions of behaviour to identify the combination of either a cavern existing in the slurry or if solids will settle, and also has the ability to be scaled to the full-scale tank. Recknagle (1999) conducted critical velocity and pressure drop measurements to examine the effect of diluting the test material.

Poloski et al. (2009) investigated the critical velocity in a non-Newtonian mixture to ensure a conservative design approach. This work mainly looked at the applicability of the stability map to identify regions of settling in laminar and turbulent regimes. Wasp and Slatter (2004) investigated the flow of fine particle metal ore slurries and their critical velocities in a homogeneous regime, seeking to refine the range of critical velocity equations; and thus proposed a new correlation based on the particle/viscous sub-layer, again for full bore pipes. Rice et al. (2017) investigated the development of time-dependent bedforms by the deposition of solid particles in two-phase flow. Several scales have been proposed to unify the observation of beds in various conduits. Rice et al. (2015) investigated the nexus between the critical deposition velocity, and the physical parameters and flow conditions of slurries, firstly at low solid volume fractions, and secondly in the limit of zero volume fraction. The two cases are analysed separately, and a general correlation in terms of the particle Reynolds number and Archimedes number is proposed for full bore pipes that is valid up to volume fractions of several per cent. Souza Pinto et al. (2014) investigated the deposition characteristics of mineral slurries and proposed a model for determining the critical velocity based on process variables which take into account the particle shape.

There have been a limited number of studies on non-Newtonian multiphase flows in open channels. Haldenwang (2003) investigated the non-Newtonian flow of carboxymethylcellulose solutions and aqueous kaolin and bentonite suspensions in rectangular open channels. An experimental database was created for non-Newtonian channel flow. Predictive models of the flow behaviour of laminar, transitional and turbulent flow behaviour were developed. Burger et al. (2010a) expanded on this study to include semi-circular, triangular and trapezoidal open channels. The flow curve for these fluids was represented by the power law, Bingham plastic and Herschel-Bulkley models. Correlations were also developed to relate the Reynolds number and friction factor of the flow based on the rheology of the test material. Burger et al. (2010b) investigated these same fluids to determine the friction factor and Reynolds number relationship for laminar flow and found a dependency on the channel geometry for the Re^{-1} relationship. Fitton (2008) found a simple method to calculate the Reynolds number at which a non-Newtonian fluid reaches laminar/turbulent transition in an open channel, along with

an estimation of head losses in the laminar, transitional or turbulent regimes, enabling the flow depth and velocity to be predicted for various fluids, flow rates and channel geometries. Spedding and Chen (1984) investigated the phenomenon of holdup in two phase liquid-gas flow, experimental studies were undertaken on horizontal, upward, and downward inclined channels. The Manning equation was found to accurately predict the holdup at low liquids rate and small downward inclination angles using previous correlations. Wang and Lam (2020) used particle image velocimetry to investigate clustering behaviour and settling velocities in turbulent open channels. A non-dimensional parameter is proposed to consider this effect and predict if the settling velocity will be enhanced or reduced. Channel flow of neutrally-buoyant rigid spherical suspensions were investigated by Lashgari et al. (2016) to understand the relationship between the particle dynamics and the mean bulk behaviour of the mixture.

The current work aims to address the two important challenges mentioned above: (1) the accuracy of flow correlations, and (2) predicting transport behaviour (i.e. the likelihood of settling). We do this through introducing a flow correlation, derived using a dimensional analysis which includes previously neglected fluid properties, as well as determining a non-dimensional settling factor to characterise the settling regime at different flow conditions. Both the flow correlation and the settling factor are tested experimentally using a gravity-driven flow of several non-colloidal suspensions in a partially-filled pipe. Our working fluids are particularly chosen to be relevant test materials for the nuclear industry as they have characteristics that are considered representative of nuclear waste slurries. As such, the work particularly supports operations within nuclear plants and associated partially filled pipelines during passive transfer operations. In these applications it is expected that fluids with less favourable transport properties will become prevalent in the future, as maximising solids loading minimises the quantity of waste that needs to be stored. Therefore a better understanding of the bulk behaviour of non-colloidal suspensions representative of nuclear slurries will help to minimise the future environmental and commercial costs of highly active liquor transfers, reducing the risk of pipe blockages during remediation and decommissioning activities. In addition, the new correlations are more widely applicable as they focus on the general fluid flow behaviour and are not limited to a specific application.

2. Experiment

2.1. Geometry and key flow parameters

Figure 1 shows the cross-section of a partially-filled cylindrical pipe, where R is defined as the pipe radius, B the length of the free surface, d the flow depth along the vertical bisector and θ is the fluid fill angle.

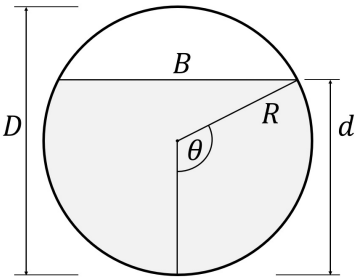

Figure 1: Pipe cross-section showing the relevant parameters associated with partially filled pipe flow, the shaded area represents the flow cross-sectional area A.

Since the flow cross-sectional area is non-circular for partially filled pipes, the hydraulic radius ($R_h = A/P_w$) is used as a characteristic length, where A is the flow cross-sectional area and P_w is the wetted perimeter. Using the geometry in figure 1, these parameters can be written as a function of fill angle (θ), as shown in equations 2 and 3,

$$A = R^2(\theta - \sin\theta\cos\theta), \tag{2}$$

$$P_w = 2R\theta. \tag{3}$$

Hence the hydraulic radius (R_h) can also be defined in terms of θ, as given in equation 4,

$$R_h = \frac{A}{P_w} = \frac{R(\theta - \sin\theta\cos\theta)}{2\theta}. \tag{4}$$

Typical to many fluid dynamics problems the Reynolds number appears as a non-dimensional group for the partially filled pipe flow problem. The characteristic length scale in the Reynolds number can have various definitions, however, for this study, the hydraulic diameter ($D_h = 4R_h$) will be used, as this is common to much of the previous work (Blinco and Partheniades, 1971; Nezu and Rodi, 1986; Ng et al., 2018). This choice of length scale has the advantage of tending to the geometric pipe diameter as the pipe becomes full. From this a hydraulic Reynolds number is defined in equation 5,

$$Re_h = \frac{4\rho U_b R_h}{\mu}, \tag{5}$$

where μ is the dynamic viscosity, ρ is the density of the fluid and $U_b = \dot{m}/\rho A$ is the bulk velocity (where $\dot{m}$ is the mass flow rate). Thus, the hydraulic Reynolds number can be defined in terms of mass flow rate ($\dot{m}$) and fill angle (θ) for a given fluid and pipe (specifically, dynamic viscosity, μ, and pipe radius, R) as given in equation 6,

$$Re_h = \frac{2\dot{m}}{\mu R\theta}. \tag{6}$$

As will be shown in §2.2 and §2.3, our experiments are designed to provide direct measurements of mass flow rate and fill angle, which can then be used along with the measured dynamic viscosity (§3.3) to enable the direct calculation of the hydraulic Reynolds number through equation 6.

As with open channel flows, the presence of a free surface in this pipe configuration means that the Froude number (Fr) is another non-dimensional group of relevance. A characteristic length scale is also required for the Froude number. Much previous work (mostly for rectangular channels) has used a mean depth ($D_m = A/B$) as this characteristic length, although there are exceptions (Chatterjee et al., 2017). For a partially-filled pipe, this length scale is problematic as $D_m \to \infty$ because $B \to 0$ as the pipe fills ($d/D \to 1$). Using a length scale that approaches infinity is not realistic, hence the hydraulic radius will be used as the length scale in the Froude number (Clausnitzer and Hager, 1997). Thus, Fr is defined as in equation 7,

$$Fr = \frac{U_b}{\sqrt{gR_h}}. \tag{7}$$

As was done for the Reynolds number, this can be written in terms of mass flow rate and fill angle for convenience. The result is equation 8,

$$Fr = \frac{\dot{m}}{\rho} R^{-\frac{5}{2}} \left(\theta - \sin\theta\cos\theta\right)^{-\frac{3}{2}} \left(\frac{2\theta}{g}\right)^{\frac{1}{2}}. \tag{8}$$

Finally, with regard to the longitudinal pipe inclination, the small angle approximation is used to relate the inclination angle of the pipe (α) to the gradient (S). By equating the sine and tangent of the inclination angle for small angles this can be expressed by the ratio of height change (Δh) along the length (L) as given in equation 9 (Chow, 1959),

$$\sin\alpha \approx \tan\alpha = \frac{\Delta h}{L} = S. \tag{9}$$

2.2. Slurry transport rig

Experiments were undertaken on the slurry transport rig (STR) located at the National Nuclear Laboratory's Workington site. The STR is a large scale non-active experimental test rig, designed for easily re-configurable pipe test sections. For this work the STR was used to study steady, fully developed, gravity driven turbulent flow in a cylindrical pipe. It was configured to supply a gravity feed of fluid to either a 0.0762 m (3 inch) nominal diameter pipeline (Line D3i) adjustable to a range of gradients from 0.5% to 1.5%, or a second pipeline parallel to first having a 0.1 m (4 inch) nominal diameter and a set gradient of 5% (Line D4i). The material of both pipelines is transparent PVC allowing for full visual observation of the fluid flow and any resulting sedimentation. A schematic of the STR is shown in figure 2.

The flow loop of the STR begins in the stock tank, this tank has a 6 m^3 capacity and can be agitated by an air sparge. A hose is then connected from the bottom of this tank into the main pump manifold where either a low or a high flow rate variable speed inverter pump can be selected by the correct valve configuration. A Grundfos CRIE 3-2 A-CA-A-E-HQQE was used for the flow rate (Q) range $1 \leq Q \leq 2.5$ m^3/hr and a BBP B50 BVGMC was used for the flow rate range $3 \leq Q \leq 12$ m^3/hr. From the pump manifold the working fluid is pumped by the outlet hose into a header tank, located 4 m above ground level. The fluid is then gravity fed vertically down through an electromagnetic flow meter into the appropriate pipeline which is pre-set at the correct gradient. On Line D3i a cylindrical plenum chamber with baffle plates is included prior to the working section to remove secondary flows due to a tight 90° bend prior to entering the working section. Both pipelines outlet into a conical receipt tank with a capacity of 0.5 m^3. When the receipt tank reaches a predetermined capacity level (set at 0.25 m^3) a constant flow rate recirculation pump engages to pump the contents of the receipt tank back into the stock tank where the process is repeated, thus allowing for a continuous feed of flow. A wash tank containing water was used to clean the pipelines of test material residue before the next test if necessary.

Control and operation of the STR is done using LabVIEW software (National Instruments). During the commissioning of the STR, the pumps where calibrated using a voltage to flow rate look-up table for a constant pressure and suction head. Hence the rig uses an open-loop program to control the flow rate by writing the calibrated voltage to pump inverters. The receipt tank sits on top of a weighbridge, the input is read by the

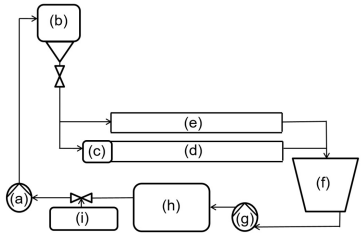

Figure 2: Flow diagram of the slurry transport rig (STR). (a) main pump, (b) head tank, (c) plenum chamber, (d) Line D3i, (e) Line D4i, (f) receipt tank, (g) return pump, (h) batch tank and (i) wash tank.

LabVIEW model, this provides a means to measure the mass flow rate being pumped around the rig. The flow rate upper limit is determined by the maximum flow rate of the recirculation pump, this is approximately 14 m^3/hr, hence the maximum flow rate of the main pump is limited to 12 m^3/hr. The flow rate range of this study was 1 to 12 m^3/hr. The stock tank has a maximum capacity of 6 m^3, but for these trials the stock tank was filled to a capacity of 4 m^3. Due to the operation of the rig, the height of the fluid in the stock tank oscillated throughout the experimental trials, the frequency of the oscillation depended upon the frequency of the engaging of the recirculation pump. The shape of the stock tank made sure that the changes in volume occurring in this tank resulted in a minimum change in fluid level meaning the pump suction head was kept relatively constant. This was confirmed as the slight change in pump suction head had a negligible effect on pump mass flow rate.

Both experimental lines where constructed using 4 m PVC pipe sections. These pieces were glued together using PVC pipe glue and the use of PVC sockets. Lines D3i and D4i are both 12 m long and contain three pipe sections and two joining sockets. Before and after the experimental pipelines 1m long pipe sections and hydraulic hoses are used to connect the two test sections to the other components of the STR. For the connection of these 1 m sections, backing clamps with stub flanges glued onto each end are used to bolt each section together with a rubber gasket fitted in between. The socket sections were used for the test sections as the socket exhibits a smoother connection than the stub flanges. Furthermore, the stub flange pipe sections are more flexible to assemble, and the smoothness of the pipe is less important in the parts of the pipeline prior to the inlet of the plenum chamber.

For this work a number of experimental instruments were used: these included a Meatest M-910 electromagnetic mass flow meter, a mass balance, draft markers and a thermocouple. The inline flow meter recorded a volumetric flow rate to an accuracy of 0.1 m^3/hr, and was monitored using the LabVIEW software, once this reading was established and the flow stabilised a mass delta was recorded over a time period of 60 seconds using the weighbridge, this gave a more precise reading of mass flow rate. Draft markers were designed specifically for the task of measuring the fluid fill level, these circular strips of paper are attached around the circumference of the pipeline and provide an indication of flow level. These draft markers were incremented in percentage fill level and degrees, where $\theta = 0^\circ$ is located at the bottom-dead-centre and $\theta = 180^\circ$ at the top-dead-centre. All draft markers were designed using CAD and accurately printed, they were aligned by placing the zero-degree line at the bottom of the pipeline. Each pipeline has a total of six draft markers located in 2 m increments between 2m and 12m along the pipe length. The full pipe length-to-diameter ratio is $L/D = 157.48$ for Line D3i and $L/D = 120$ for Line D4i. The first draft marker located at 2 m was largely unused for data collection purposes as $L/D < 30$ at this location. Therefore the second marker, located at 4 m downstream of the test section inlet was the first marker used to record measurements. This is located at $L/D = 52.5$ for Line D3i and $L/D = 40$ for Line D4i. It was deemed that this ratio gave a sufficient development length for the fluid entering the pipe working section. Lastly, a thermocouple was placed on the stock tank outline isolation valve. The temperature of the working fluid was logged during the trial to enable accurate calculation of fluid viscosity (which is dependent on temperature). Viscous heating is so low that no significant change in temperature was observed during an individual trial. The data collected for this paper was collected over a 12-month period, with a working fluid temperature ranging from $14 \leq T \leq 20^\circ$C.

2.3. Experimental procedure

Prior to the start of any experimental work, the pipe was set to the required gradient. A tape measure was used to measure the location of the pipe stand at a set position from the pipe inlet as well as the height of each pipe stand. A digital spirit level was used to make sure the ground was level, this was calibrated on a drilling platform known to be horizontal. The uncertainty in the setting of each individual pipe was estimated to be ±5mm, resulting in a potential error in the gradient of $< 0.1\%$. Pipe stands were placed every 2 m along the length of the pipe to avoid sagging. Once the gradient was set the stock tank was agitated with the air sparge

pole for a minimum of 15 minutes (if the rig was running with only water this process was unnecessary and omitted). Sufficient agitation was achieved by discharging air at 7 bar into the bottom of the stock tank. Measurements of fluid temperature and atmospheric pressure were taken. Once this was completed and the mixture homogenised, the valves were opened and a flow rate on the main pump was selected, initiating the flow of fluid through the working section and into the receipt tank. Once the receipt tank weighbridge recorded an increasing mass of fluid in the tank, the mass change was measured over a one-minute period. A plot of the mass of fluid in the receipt tank versus time was shown live on the LabVIEW graphical user interface (GUI). A line of constant gradient showed the flow was steady, which was invariably achieved after only a few seconds of selecting a flow rate. The angle (θ) was measured on five of the draft markers (at 4 m from the inlet of the working section and at every 2 m location downstream) in order to record the fill-height of the fluid in the pipe. Typical fluctuations in these readings ranged from $\approx 0^\circ$ at low flow rates to $\pm 3^\circ$ at the highest flow rates. Finally, the observed settling regime was recorded. Typically, this process would take approximately 10 minutes before a new flow rate was selected and the same process repeated. A standard trial would start with $Q = 1$ m^3/hr and increase in increments of 0.5 m^3/hr to $Q = 12$ m^3/hr, then a repeat of the flow rate range would be conducted in reverse, starting at the higher flow rate and decreasing in the same increments to the lowest flow rate. It was found the results were independent of the flow rate being incrementally increased or decreased. This procedure was repeated three times for five different working fluids (described in §3) and at least three different gradients. Uniform flow was observed along the length of the working section, so (for each flow rate) the five draft marker measurements were averaged, resulting in a single θ measurement. From this a range of parameters typical to partially filled pipes can be calculated using the geometry shown in figure 1 as demonstrated in §2.1.

3. Test materials

The test materials in this study were water (mainly as a reference) along with two different non-colloidal suspensions. The solid particles in these aqueous suspensions were calcium carbonate (chalk) and barium sulphate (barytes), each at two different concentrations. These materials were chosen to be consistent with non-active nuclear waste test materials (McArthur et al., 2005; Paul et al., 2013; Dunnett et al., 2016). The concentrations of chalk and barytes were chosen to align with typical concentrations being transferred around nuclear facilities. For this study, water and four different working fluids (two different materials each at two concentrations) were used as shown in table 1. The density of the raw materials was measured and matched the manufacturer's specifications. For calcium carbonate this was 2700 kg/m^3 and for barium sulphate this was 4400 kg/m^3. Both test materials were each mixed with water in accordance with 40 and 60 kg of the solid test material being present in a mixture of 1 m^3. This can be compared to a w/w concentration by dividing the solid mass by the mass of the remaining water in the 1 m^3 mixture. A volume ratio can be found by dividing the volume of solid by the volume of water in the 1 m^3 mixture. Finally, a slurry density can be found by summing the mass of the solid and remaining water and then dividing by 1 m^3. Several methods to characterise the physical properties of these suspensions were undertaken, these methods were consistent with a study by Paul et al. (2013) looking at the characterisation of highly active nuclear waste simulants.

3.1. Particle size

The Malvern Instruments Mastersizer 3000 was used to obtain a particle size distribution (PSD) for the two test materials. The samples were sized using a wet dispersion unit (Hydro EV), with refractive indices of 1.33 for water, 1.60 for chalk and 1.64 for barytes (Lide, 2007). Ten measurements were taken for both dry chalk and barytes, the Mie scattering model was used to obtain an average particle size distribution of these samples. This was then repeated for hydrated samples taken from the STR. It was found that the peak value for chalk reduced by 2.6 μm with barytes having a negligible difference. The results of the PSD are shown in figure 3. Nominal values of 12 μm for chalk and 17 μm for barytes, which correspond to the peaks of the PSD for the hydrated samples, were used to characterise the particle diameters when required.

3.2. Settling velocity

A settling velocity for each of the four suspensions was obtained by performing static settling tests. The mixture was made up in a 250 ml measuring cylinder and agitated sufficiently to create a homogeneous suspension. The measuring cylinder was then left at rest to allow the solid particles to settle. A clear interface between the settling solid-liquid mixture and the clear water supernatant formed and the descending height of the interface was recorded at frequent time intervals (Kökpınar and Göğüş, 2001). The procedure was performed for all four working fluids and repeated three

Label	Test Material	Concentration (kg/m^3)	Mass concentration w/w (%)	Volume concentration (solid:liquid)
Water	Water	N/A	N/A	N/A
C40	Chalk	40	4.06	1:66.5
C60	Chalk	60	6.14	1:44
B40	Barytes	40	4.04	1:109
B60	Barytes	60	6.08	1:72.3

Table 1: Test materials and concentrations.

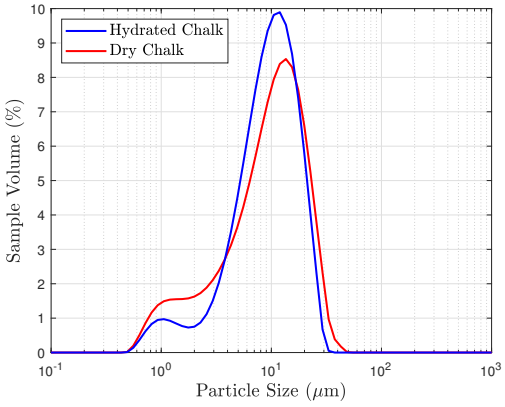

(a)

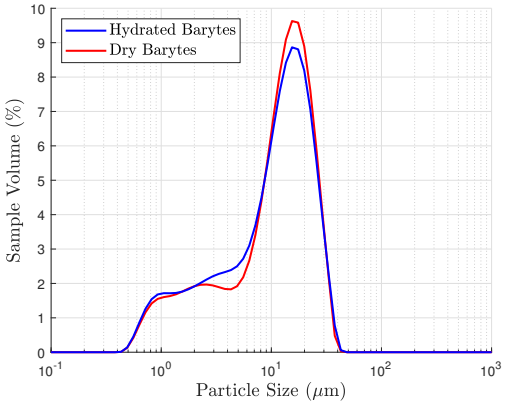

(b)

Figure 3: Particle size distributions of hydrated and dry samples of (a) chalk and (b) barytes.

times for each. As seen in figure 4, initially a linear decrease in the height of the interface with time was observed, followed by an asymptotic behaviour due to the hindered settling effect of the higher concentration mixture. To find the unhindered settling flow rate, a linear fit of the initial settled bed height readings, recorded over the first 5 minutes, was performed and the gradient of this line gave the settling flow rate. The R-squared value for the linear fit was calculated in order to be sure of the accuracy of the linear fit, all the working fluids have an R-squared value above 0.99 as shown in table 2.

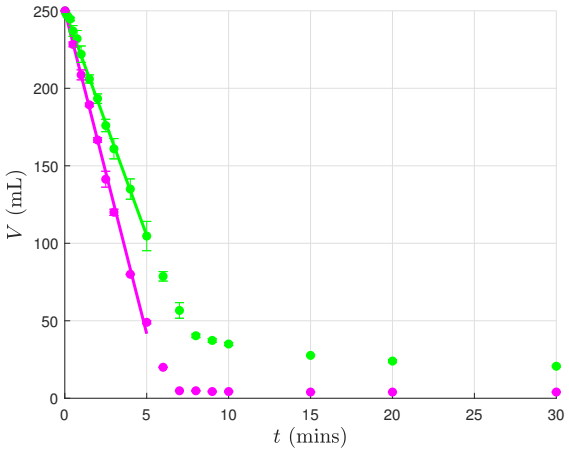

(a)

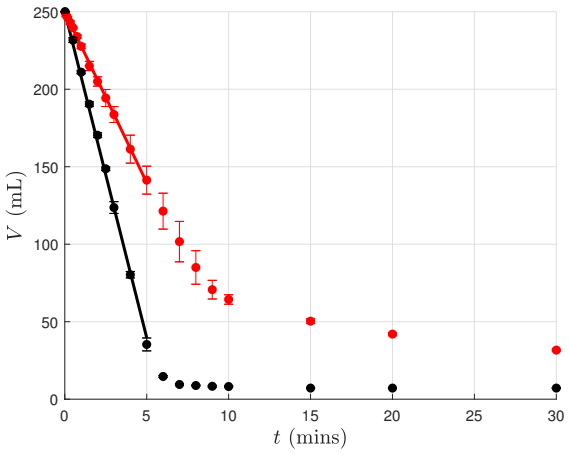

(b)

Figure 4: Average particle settling volume verses time: (a) C40 (green) and B40 (pink) and (b) C60 (red) and B60 (black). Error bars indicate one standard deviation from the mean. Solid lines indicate a linear fit for the initial settling rate, which is used to calculate the settling velocity.

Once the settling flow rate was known, the settling ve-

locity v_s can be found by dividing the settling flow rate by the cylinder cross-sectional area (which was constant for each experiment). The two barytes concentrations have very little difference in settling rate values (< 5%) between them, it appears the higher density of the solid barytes is the dominant factor. However, there is a difference in the settling velocity for the two chalk concentrations, with the lower concentration having approximately a 30% faster settling velocity than the higher concentration. This can be explained by the low density of the solid chalk being more affected by the particle to particle interaction during the settling process (Cheng, 1997). A Stokes number for the settling particle can be calculated using the definition stated in equation 10 (Swaminathan et al., 2006),

$$St = \frac{\rho_p v_s d_p}{\mu_w}, \tag{10}$$

where ρ_p is the test material particle density, d_p particle diameter and μ_w the viscosity of water. A summary of the measured mixture density, particle size, settling velocity and Stokes number is shown in table 2.

3.3. Rheology

The Anton Parr MCR302 rotational rheometer was used to obtain the rheological properties of the working fluids. Measurements were taken using a cone and plate geometry with a 1° cone angle at 20°C. A particular shear profile (shown in figure 5) was developed for the rheological characterisation of the working fluids to avoid settling and ensure measurements of the homogeneous suspension of the mixture could be made. A pre-shear of 30 seconds is first applied at a high shear rate of $1000s^{-1}$. At this high shear rate sufficient agitation was provided to the sample to avoid a solid bed forming. Next the shear rate was dropped to $100s^{-1}$ and held for 10 seconds before a measurement was taken, then the shear rate was increased back to $1000s^{-1}$ to re-suspend any settled solids, before the whole process was repeated for incrementally increasing lower shear rates. The viscosity values at all the $1000s^{-1}$ points show a negligible difference between them (figure 6), hence we are confident that the high shear rate pulses are sufficient at keeping a homogenised sample.

A non-Newtonian shear thinning relationship for the non-colloidal suspensions is shown in figure 6, and is consistent with the literature (Turian et al., 1997; Paul et al., 2013). Error bars show the maximum and minimum values at a particular shear rate. This variation is attributed to errors when sampling causing differences in concentration. A power law model (equation 11) can be fitted for each of the test materials (Barnes et al., 1989),

$$\tau = K\dot{\gamma}^{n_p}. \tag{11}$$

The parameters and accuracy of the fits are defined and displayed in table 3. A power law model was used because the data in the shear rate range of interest clearly show a power-law form (and the R-squared values of the fit are high). Other studies of rheological properties have favoured a Herschel-Bulkley model, but these studies tend to have much higher solid concentrations (> 10 wt%) (Turian et al., 1997; Nguyen et al., 2006; Dunnett et al., 2016). For our fluids (at the lower solid concentrations) the yield stress is not relevant to the rheological characterisation in the shear rate range measured and therefore to include it in the model would be inappropriate. The calculation of the Reynolds number for shear-thinning fluids is not straightforward as the shear rate (and therefore viscosity) varies throughout the flow field. To define a Reynolds number a calculation of the mean wall shear stress (τ_w) for each of the trials was made using measurements from the pipe flow experiment and equation 12,

$$\tau_w = \rho g R_h S, \tag{12}$$

which is a function of flow depth and based on a mass balance of the fluid (Chow, 1959). Using the power law parameters, a characteristic shear rate ($\dot{\gamma}_c$) can be calculated using equation 13,

$$\dot{\gamma}_c = \left(\frac{\tau_w}{K}\right)^{\frac{1}{n_p}}. \tag{13}$$

Once the characteristic shear rate has been found the power law model can be used to calculate the related dynamic viscosity (μ),

$$\mu = K\dot{\gamma}_c{}^{n_p-1}, \tag{14}$$

which can be used in the calculation of Re.

As an indication of the shear rate range observed in the pipe flow experiments, the highest and lowest shear-rate values for line D3i are shown by the diamonds in figure 6. It is noted that the highest shear rate in some of the experiments is higher than that measured on the rheometer (this was also the case for line D4i). Therefore we need to extrapolate the power law fit to higher shear rates in order to calculate the characteristic viscosity for these experiments (to enable calculation of Re_h). However this only resulted in a small change in viscosity ($\approx$ 1 mPa s lower) compared to the viscosity at the highest shear rate reachable on the rheometer. Given

Fluid	Mixture density (kg/m^3)	Particle size (μm)	Settling velocity (mm/min)	R-squared (settling rate fit)	Stokes number
C40 (green)	1025	12	28.99	0.9982	0.0157
C60 (red)	1038	12	22.05	0.9994	0.0119
B40 (pink)	1031	17	41.67	0.9969	0.0519
B60 (black)	1046	17	42.06	0.9979	0.0524

Table 2: Mixture density, particle size, settling velocity and Stokes number for each of the working fluids.

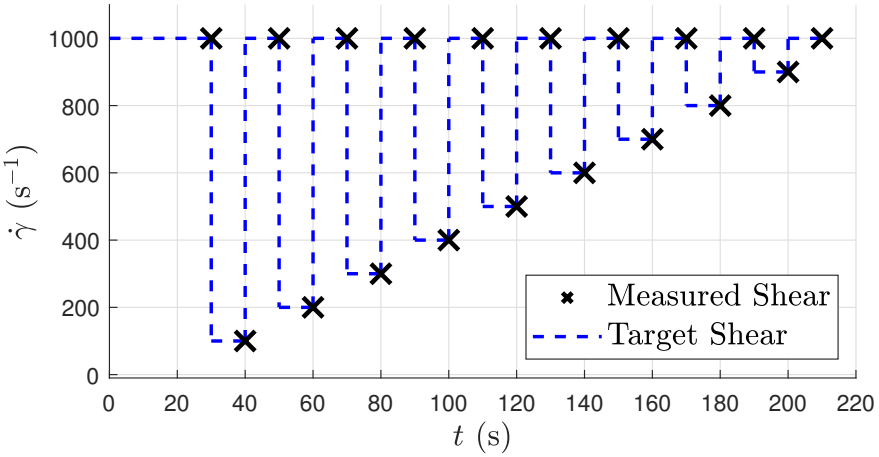

Figure 5: Shear rate (s^{-1}) as a function of time (t) showing the shear profile (blue line) and the points of measurement (black circles).

the uncertainty in estimating an appropriate characteristic shear in such a flow, any loss of accuracy introduced by this extrapolation is considered to be negligible. The viscosity values of this dataset are consistent with those by Rice et al. (2020), who used an in-line acoustic technique to measure the rheology of calcium carbonate and barium sulphate at volume fractions of 10%, 15% and 20%. Rice et al. (2020) also reported low yield stresses would be present in concentrations of the magnitude in this study (< 0.01 Pa).

4. Flow correlations

Experiments were conducted and data was collected for Reynolds numbers in the range of $2 \times 10^3 \leq Re_h \leq 1.1 \times 10^5$, and Froude numbers in the range of $1.1 \leq Fr \leq 4.4$. A summary of experimental trials conducted for each working fluid, pipeline and pipe gradient alongside the calculated range of the parameters d/D, Re, Fr is shown in table 4. Observed settling regimes are reported in the last column, these are marked by H for *homogeneous suspension*, P for *dynamic pathlines*, M for *a moving bed* and S for *a settled bed*. These regimes are explained in more detail in §5. It demonstrates the variety of combinations of pipe inclinations and diameters, as well as fluids, that the current dataset contains. This variety is important in order to strengthen the broad applicability of any flow correlations tested using this dataset.

4.1. Velocity

One of the quantities that is of primary interest to anyone designing open channel or partially filled pipe flows is the average (or bulk) velocity, because achieving an appropriate velocity can be crucial to the successful and efficient operation of the channel or pipeline. This can be for many reasons, but using the context of slurries as an example, it is a determining factor in the transport of sediments and whether they are effectively transported or settle in the pipe. In this work we are particularly interested in predicting the flow in partially filled pipelines of slurry materials (non-colloidal suspensions). Our approach is based on dimensional analysis in an attempt to develop a correlation that is more universal, rather than simply deriving an equation specifically for our application. As the Manning equation works very well, particularly for water flows, we use it as our starting point. One of the aspects of the

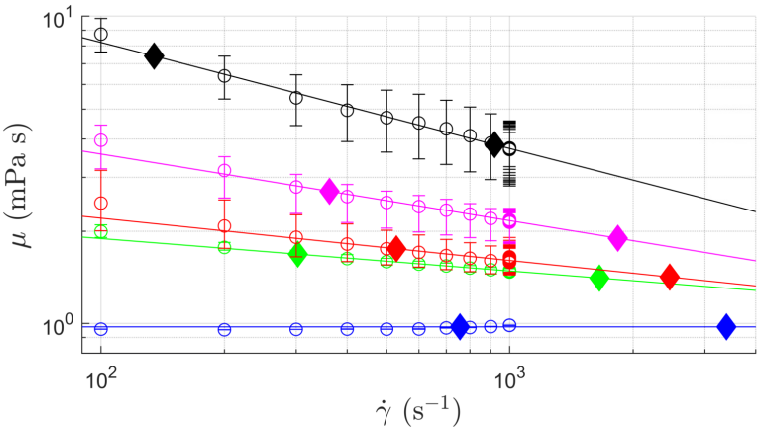

Figure 6: Dynamic viscosity (μ) as a function of shear rate (s^{-1}) for the five different working fluids taken at a temperature of 20°C. Water (blue), C40 (red), C60 (green), B40 (pink) and B60 (black). Circles represent the mean with error bars showing the maximum and minimum values. Solid lines are power law fits described by equation 11, with parameters in table 3. Diamonds indicate the lower and upper characteristic shear rates of experimental data on line D3i.

Fluid	Flow consistency index – K (mPa s^{n_p})	Flow behaviour index – n_p	R-squared
C40 (green)	3.0790	0.8943	0.9999
C60 (red)	4.1640	0.8620	0.9983
B40 (pink)	9.7280	0.7825	0.9993
B60 (black)	39.840	0.6570	0.9985

Table 3: Power-law parameters for working fluids.

equation that attracts particular attention is the n coefficient. It is doubtful that it solely relates to the roughness of the duct wall as not only does that not make dimensional sense, but often different values of n are given for pipes made of different materials when both materials are hydrodynamically smooth (Barr et al., 1986). Using the Manning equation to empirically fit our data for each of the different working fluids unsurprisingly yields a different value of n for each material, the values of which are shown in table 5.

The value of 0.009 is recorded in the literature as a value representative of water on smooth PVC (Bishop and Jeppson, 1975), which is the material our pipeline is constructed from. The values in table 5 are not far from this value, especially for water. However, our fitted values do appear to be dependent on the properties of the test material and not just the roughness of the channel wall. The goodness of the fits (R-squared values in table 5) indicates that the form of the equation (i.e. exponents of both R_h and S) appear to be robust. It can therefore be concluded that other parameters are implicit in the n value. We use this information to form a new correlation where the relationships to R_h and S are carefully preserved, but new parameters are introduced in place of the single coefficient (n).

We hypothesise that the relevant parameters to replace n are the acceleration due to gravity (g), the fluid density (ρ) and dynamic viscosity (μ). Given that the Manning equation applies to water flows on Earth it is not particularly surprising that the gravitational acceleration and fluid properties were not specifically considered in its formulation. However, it seems undeniable

Fluid	Pipeline	S (%)	d/D (%)	Re_h	Fr	Settling regimes
Water	D3i	0.5	38 - 72	$3.3 \times 10^3 - 5.7 \times 10^3$	1.24 - 1.39	N/A
Water	D3i	1	30 - 79	$3.1 \times 10^3 - 8.1 \times 10^3$	1.66 - 1.89	N/A
Water	D3i	1.5	27 - 71	$3.3 \times 10^3 - 9.5 \times 10^3$	1.99 - 2.27	N/A
Water	D4i	5	9 - 28	$1.4 \times 10^4 - 1.1 \times 10^5$	2.71 - 4.18	N/A
C40	D3i	0.5	20 - 72	$7.7 \times 10^3 - 3.9 \times 10^4$	1.09 - 1.41	M, P, H
C40	D3i	1	18 - 80	$8.7 \times 10^3 - 5.9 \times 10^4$	1.34 - 1.88	P, H
C40	D4i	5	8 - 31	$1.1 \times 10^4 - 9.9 \times 10^4$	2.96 - 4.35	H
C60	D3i	1	20 - 80	$9.3 \times 10^3 - 5.5 \times 10^4$	1.40 - 1.86	P, H
C60	D3i	1.5	19 - 70	$9.9 \times 10^3 - 6.6 \times 10^4$	1.45 - 2.17	P, H
C60	D4i	5	9 - 32	$1.3 \times 10^4 - 9.8 \times 10^4$	3.13 - 3.94	H
B40	D3i	1	21 - 86	$5.3 \times 10^3 - 3.7 \times 10^4$	1.15 - 1.73	S, M, P, H
B40	D3i	1.5	16 - 71	$4.5 \times 10^3 - 4.9 \times 10^4$	1.29 - 2.17	S, M, P, H
B40	D4i	5	9 - 32	$7.8 \times 10^3 - 7.9 \times 10^4$	2.53 - 3.75	P, H
B60	D3i	1	21 - 89	$2.0 \times 10^3 - 1.6 \times 10^4$	1.13 - 1.72	S, M, P, H
B60	D3i	1.5	19 - 74	$2.5 \times 10^3 - 2.4 \times 10^4$	1.28 - 2.00	S, M, P, H
B60	D4i	5	10 - 33	$4.3 \times 10^3 - 5.1 \times 10^4$	2.78 - 3.57	P, H

Table 4: Summary of experimental trials for each working fluid, pipeline and gradient with the range of d/D, Re, Fr and settling regimes.

Fluid	Fitted n	R-squared
Water	0.0092	0.8892
C40	0.0094	0.9654
C60	0.0095	0.9654
B40	0.0101	0.9584
B60	0.0105	0.9562

Table 5: Fitted Manning roughness coefficient values for each working fluid.

that each would play a key role in the flow behaviour. In doing this we are actually neglecting any dependence on wall roughness and as such are deriving a correlation for hydrodynamically smooth conduits. Although we are still confined to Earth and cannot test any dependence on g, we retain it because we wish to preserve the true dimensions. For the fluid properties, noting that we have no other quantities that have dimensions of mass, we can safely just use the kinematic viscosity ($\nu = \mu/\rho$). Dimensionally n can be replaced by ν, g, and in addition we include a non-dimensional factor, c, which we suppose to be constant, giving equation 15,

$$\frac{1}{n} = c\frac{g^{\frac{5}{9}}}{\nu^{\frac{1}{9}}}. \tag{15}$$

Performing dimensional analysis using all the parameters in this new system yields three non-dimensional groups: Re, Fr and S. Within these groups, ν only appears in the Reynolds number and g only appears in the Froude number. Hence (with reference to equation 15), equation 16 can be derived as a non-dimensional replacement to the Manning equation,

$$Fr^{\frac{10}{9}} = cS^{\frac{1}{2}}Re_h^{\frac{1}{9}}. \tag{16}$$

All the parameters in equation 16 (including c) are non-dimensional and the value of c can be found empirically using the measured Froude and Reynolds numbers for each corresponding channel slope. Figure 7 shows the calculated factor, c, plotted against Reynolds number, Froude number and depth, where each data point is coloured by the working fluid. It is clear that for all working fluids and Re tested, the value of c is roughly constant. It is certainly not possible to identify any functional dependence on any of the flow parameters, and the five different working fluids exhibit the same degree of scatter with no distinct separation between them. The probability density function of c is shown in figure 7d and is normally distributed. This suggests that the variation in the value of c is due to measurement error, which is equally distributed throughout the working fluids. The two concentrations of barytes formed settled beds at low Reynolds numbers (as will be shown in §5), as a result, the recorded hydraulic radius was not representative of the flow cross-sectional area, and the flowing fluid would be of a more diluted form (with lower density and viscosity). In these situations the values of R_h and ν are essentially incorrect, hence these

data points (shown in the red circle in figure 7) are not reliable, and we observe they are some of the furthest from the mean value of c.

Equation 16 can be applied to the data of other studies, as shown in the inset in figure 7 (a). These studies are for gravity driven water in either a circular, rectangular, or trapezoidal channel. Nezu and Rodi (1986) is in closest agreement with this study's mean c value (a difference of 2%), with all their data points falling within one standard deviation of our mean value. Tominaga et al. (1989) has an error of 4.3%, having a scatter of values between $5.1 < c < 5.5$. Blinco and Partheniades (1971) has a similar error of 5% with measurements showing scatter similar to that of our data ($5.2 < c < 5.8$). Knight and Sterling (2000) and Bishop (1978) fall near the lower one standard deviation line with mean errors of 7.5% and 8.7% respectively. The average value of c for all these other studies combined differs by 3.6% to that obtained from our data alone. The overall conclusion from testing our equation using other data is that the error and scatter is commensurate with the error and scatter in our data, which we largely attribute to experimental uncertainties. Therefore, to within the accuracy of our experiments and the experiments of these previous works, equation 16 appears to be valid, with a constant value of $c \approx 5.6$. Given that the data encompasses a few different working fluids, many different fill-heights, numerous pipe diameters, and several different duct cross-sectional geometries, this is a rather pleasing level of agreement.

The ability of this correlation to reliably predict an estimate of the velocity in a pipeline can be tested by rearranging equation 16 into a velocity form, using the definitions of Reynolds and Froude number in equations 5 and 7,

$$U_b = \frac{c}{(4\nu)^{\frac{1}{9}}} g^{\frac{5}{9}} R_h^{\frac{2}{3}} S^{\frac{1}{2}}. \tag{17}$$

For each working fluid the bulk velocity was calculated for the range of fill levels, $0 \leq \theta \leq \pi$, using the appropriate kinematic viscosity and channel slope. This bulk velocity term was then used in the standard Reynolds number definition; hence a correlation of fill height verses Reynolds number can be shown by the solid lines in figure 8. The same method can be done for the original Manning equation and this is shown by the dashed lines, the presence of the fluid properties in the new equation is the primary reason for the offset between the Manning curves and our Fr–Re–S–correlation (Fresco). It can be readily observed that this offset increases as the physical properties of the working fluid diverge from those of water; water being the fluid the original Manning equation was based on. As discussed in §2.1 we can calculate the fill-height (d/D) and Re in our experiments from purely experimental observations. These are plotted in figure 8 as data points for each of the slopes and pipe diameters. It is evident that Fresco works well for all the data we obtained and whilst the predictions are similar to the Manning equation for water, the Fresco predictions are far superior for the other working fluids. Overall the agreement between the experiments and the Fresco predictions is excellent and any differences are well within the experimental uncertainty of the measurements.

4.2. Friction factor

The Darcy friction factor (f_D), in head loss form appropriate for gravity-driven flow, is given in equation 18,

$$f_D = 2\frac{\Delta h}{L}\frac{gD_h}{U_b^2}. \tag{18}$$

Using equation 9 and noting that $D_h = 4R_h$, equation 18 can be rewritten to express the Darcy friction factor as a function of Froude number (equation 7) as shown in equation 19.

$$f_D = 8S\frac{gR_h}{U_b^2} = \frac{8S}{Fr^2} \tag{19}$$

A plot of friction factor against Froude number is shown in figure 9. The experimental data for all fluids, pipe diameters and gradients agree very well with equation 19. It is clear that the channel slope provides a fundamental link in the relationship between these parameters and also provides a method of validating the uniformity of the channel slope. In addition to the current dataset, data from Knight and Sterling (2000) and Yoon et al. (2012) are also included. These are also in broad agreement with equation 19 for their respective channel slopes.

In many areas of pipe flow design the Moody diagram is an important reference and the Blasius correlation ($f_D = 0.316Re^{-\frac{1}{4}}$) exists for an approximation of friction factor for full bore turbulent pipe flows (LaViolette, 2017). A plot of friction factor against Reynolds number using our data is shown in figure 10 with the Blasius correlation shown by the black dashed line. The data points appear to stray from Blasius and this is likely due to the intrinsic difference between full bore and partially filled pipe flow and the fact that the slope of the channel is not considered by Blasius. Using Fresco (equation 16) and substituting into equation 19, a new expression for friction factor containing both c and S can be found as shown in equation 20,

$$f_D = 8c^{-\frac{9}{5}} S^{\frac{1}{10}} Re_h^{-\frac{1}{5}} = 0.36 S^{\frac{1}{10}} Re_h^{-\frac{1}{5}}. \tag{20}$$

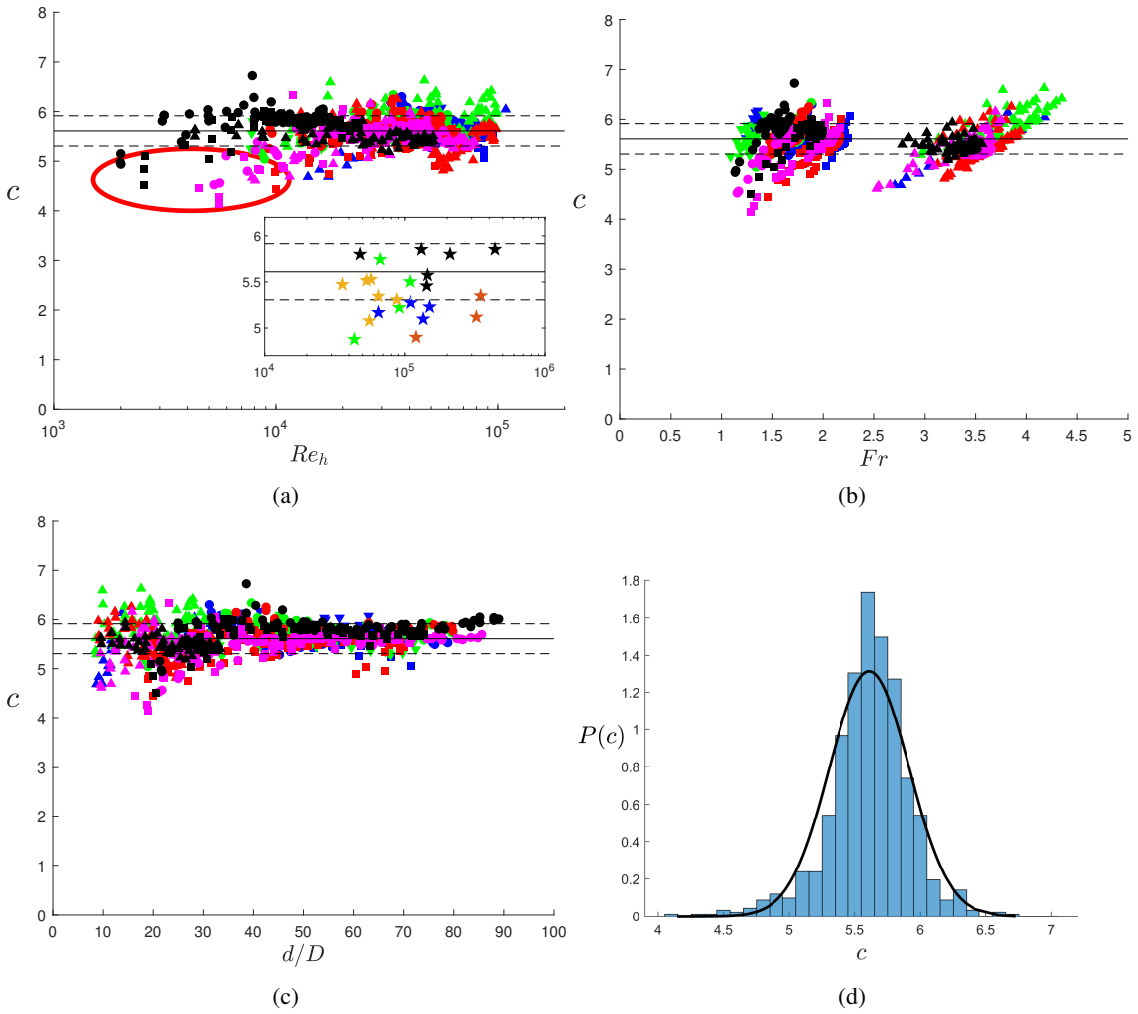

Figure 7: The non-dimensional factor (c) as a function of (a) hydraulic Reynolds number, (b) Froude number and (c) flow depth for all working fluids. Water (blue), C40 (green), C60 (red), B40 (pink) and B60 (black). Inset of (a) shows data from other studies represented by: blue stars Knight and Sterling (2000), black stars Nezu and Rodi (1986), green stars Blinco and Partheniades (1971), brown stars Bishop (1978) and gold stars Tominaga et al. (1989). Solid line represents the average of this study's data sets (c = 5.6), the dashed lines represents one standard deviation from this average. (d) Probability density function of scaling factor (c) for all data points, evaluated with intervals of 0.1. Black line is a Gaussian distribution with the same mean and standard deviation of c for reference.

The addition of these terms using Fresco results in a much improved f–Re_h correlation in comparison to Blasius (as can be observed in figure 10), although it is admittedly still not perfect. The largest improvements are observed for the experiments where the slope of the pipe is greatest, which is to be expected. The data points at low Reynolds numbers which appear to fall away from this new correlation are occurring in regimes of high sedimentation and suffer the same reliability issues highlighted in §4.1.

5. Transport behaviour

Of paramount importance to many applications, but especially in the flow of nuclear slurries, is the effectiveness of the flow in transporting solid particles along the pipeline without them settling. Whilst a high solids loading is desirable to minimise the quantity of waste, this increases the likelihood of the solids settling, which can lead to serious failures, such as blockages, which require expensive and difficult remediation. It is highly preferable to design the pipeline, and the operating conditions associated with it, such that solid matter is transported along the pipe and does not settle. However, the

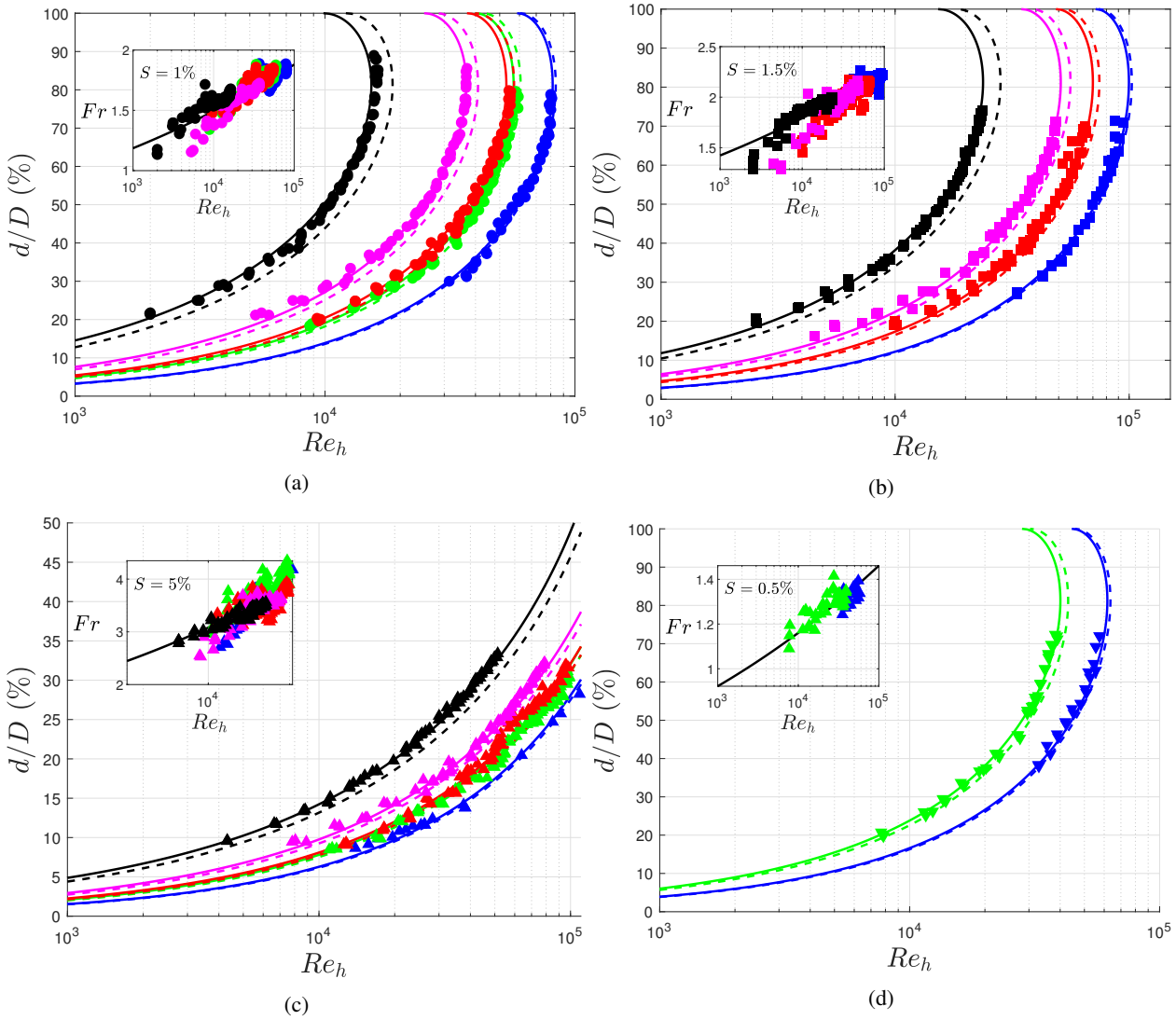

Figure 8: Non-dimensional flow depth as a function of hydraulic Reynolds number. Colours represent working fluids: water (blue), C40 (green), C60 (red), B40 (pink) and B60 (black). (a) $S = 1\%$ on D3i (circles), (b) $S = 1.5\%$ on D3i (squares), (c) $S = 5\%$ on D4i (triangles), and (d) $S = 0.5\%$ on D3i (inverted triangles). Solid line represents Fresco (equation 16) and dashed line represents Manning (equation 1 with $n = 0.009$) coloured by working fluid. Insets show the variation of Froude number with Reynolds number for the appropriate gradient as described by equation 16.

prediction of such satisfactory operating conditions is difficult. This is one reason why the Fresco flow correlation presented in §4 is useful, because it can be used to predict the bulk velocity of the flow in the pipe from known parameters, and the velocity is a key parameter in determining whether solids will be transported effectively.

There are, of course, more parameters involved in the settling problem, and that is the focus of this section. Using our experimental database we find a simple non-dimensional number, calculable from commonly known parameters (the fluid properties and bulk velocity), which provides a reliable prediction of the settling regime seen in the pipe. Thus, it (combined with Fresco) provides a simple method of determining a bulk velocity for the effective transportation of a given slurry.

5.1. Settling regimes

Four distinctly different settling regimes were observed across our range of experimental tests (see table 4 for experimental conditions). These regimes are outlined below and illustrated in figure 11.

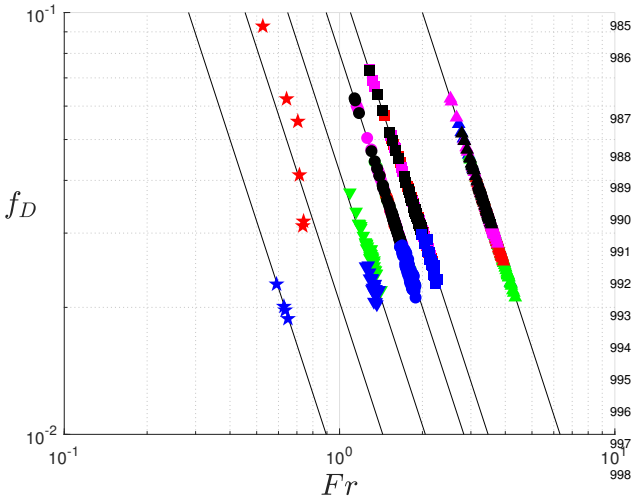

Figure 9: Darcy friction factor as a function of Froude number for a pipe gradient of 0.5% (inverted triangles), 1% (circles), 1.5% (squares) and 5% (triangles) for D3i (inverted triangles, circles and squares) and D4i (triangles). Data from other studies is represented by: blue stars Knight and Sterling (2000) and red stars Yoon et al. (2012). Solid lines represent equation 19.

1. *Homogeneous suspension* is where the solid particles are uniformly distributed throughout the liquid phase of the mixture with a negligible gradient in concentration, here no separation into solid particles and supernatant is visible, (figure 11a).
2. *Dynamic pathlines* are thin lines of moving particles forming near the pipe wall, these lines tend to align with the streamwise direction and move at a velocity similar to the average fluid velocity (figure 11b). Dynamic pathlines grow in intensity until they become a moving bed.
3. *A moving bed* consists of a thick bed of solid material moving at a similar velocity to the liquid phase, a diluted supernatant is visible above the moving bed, (figure 11c).
4. *A settled bed* forms at the base of the pipe when a moving bed becomes stationary, this has a clear solid to liquid interface and the liquid phase flows down the pipeline above the stationary bed, (figure 11d).

These four regimes are similar in definition to those outlined in the literature (Doron et al., 1987; Peker and Helvaci, 2011; Wells et al., 2011) but for a partially-filled instead of a full-bore pipe. All these settling regimes reached a steady state apart from the settled bed. In the settled bed regime, the bed depth increased slowly from an initial value of zero to form a non-uniform bed with varying bed height (Rice et al., 2017). A final measurement was taken after 20 minutes before the experiment was abandoned to avoid large deposits of sediment in the pipeline.

5.2. Settling factor

There are examples in the literature where a dimensionless parameter has been used to measure the intensity of the settling in a fluid flow. A non-dimensional velocity parameter can be used to do this (Yu et al., 2004), however due to the wide range of settling velocities in this study, another parameter which encompasses more properties, including the particle density, is necessary. A single dimensionless parameter to quantify and predict the settling was found, similar to the gravity yield parameter for tank settling and bed clearance (Adamson, 2011). We term this the settling factor (and use the alternative form of the Greek sigma, ς) as shown in equation 21,

$$\varsigma = \frac{\rho_p - \rho_f}{\rho} \frac{\nu_f}{U_b d_p} = \frac{\rho_p - \rho_f}{\rho} Re_p^{-1}. \quad (21)$$

In equation 21, ρ_p is the density of the solid particle, ρ is the density of the working fluid (i.e. solid and liquid combined, as defined previously), ρ_f and ν_f are the density and kinematic viscosity of liquid (water in our experiments), U_b is the flow bulk velocity, and d_p is the particle diameter. This form of settling factor essentially involves a term related to the specific gravity of the particles, and a second term which forms a Reynolds number (Coulson et al., 1993). The term related to the specific gravity is large for dense particles that will tend to settle quickly. We have chosen this form rather than the specific gravity itself because it means that buoyant particles (less dense than the surrounding fluid) would give $\varsigma < 0$ (neutrally buoyant $\varsigma = 0$), which seems sensible. However, we have not tested any buoyant particles to confirm this wider applicability. The Reynolds number (Re_p) is a particle Reynolds number because the length scale is the particle diameter and not the hydraulic radius (so $Re_h \neq Re_p$). Also, the viscosity of the liquid is used and not the viscosity of the homogeneous suspension (Miskin et al., 1996). However, it is the bulk velocity of the flow down the pipeline that is used, which is obtainable using Fresco. A high Re_p will act to sweep the particles along the pipe with the flow, and as such a high Re_p leads to less settling. Thus, the settling factor (ς) is a simple mathematical representation of the competition between the density-driven settling of particles and the action of the bulk flow to transport them down the pipeline. A high value of ς indicates a higher intensity of settling, hence the name, settling factor.

The settling factor was calculated for each measurement in our entire data-set and plotted against hydraulic

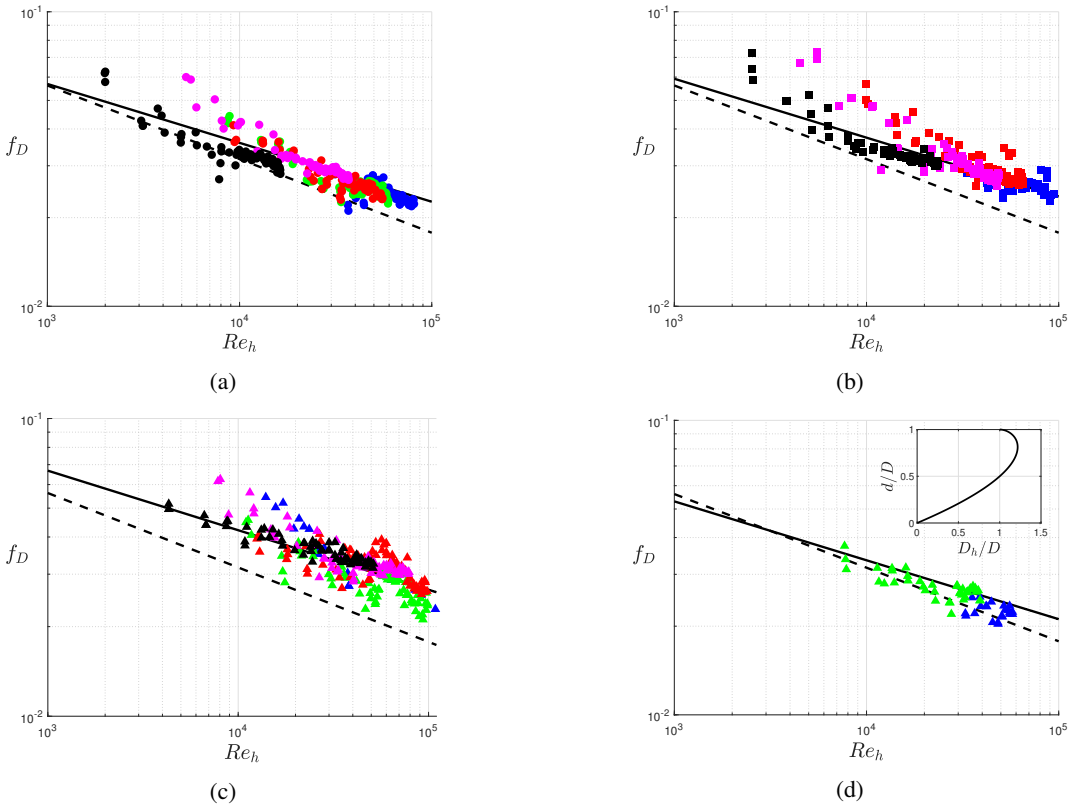

Figure 10: Darcy friction factor as a function of hydraulic Reynolds number. Colours represent working fluids: water (blue), C40 (green), C60 (red), B40 (pink) and B60 (black). (a) $S = 1\%$ on D3i (circles), (b) $S = 1.5\%$ on D3i (squares), (c) $S = 5\%$ on D4i (triangles), and (d) $S = 0.5\%$ on D3i (inverted triangles). Solid lines represent equation 20, dashed lines represent the Blasius correlation ($f_D = 0.316Re^{-\frac{1}{4}}$). Inset of (d) shows the variation of flow depth d/D with hydraulic diameter D_h/D.

Reynolds number in figure 12. The data points have been coloured according to the settling behaviour observed in the pipeline. These are homogeneous suspension (blue), dynamic pathlines (red), moving bed (green) and settled bed (black). There is a general trend where increasing Re_h results in a lower settling factor, which is to be expected. However, more stark, is the separation of the four settling regimes with settling factor. It is clear that the ability to calculate the settling factor (ς) in equation 21 is all that is needed to have a good prediction of the settling regime that would occur in that pipeline (regardless of the specific Re_h). Horizonal lines of constant settling factor have been drawn at the boundaries between the different sedimentation regimes. The ς-values of these boundary lines have been calculated by finding the average between the lowest settling factor in the upper regime and the highest settling factor in the lower regime. A summary of the values for each boundary is shown in table 6. There are slight overlaps at the boundaries between the dynamic pathlines flow regime and the two neighbouring regimes (moving bed and homogenous suspension). This could be due to the transition between these settling regimes not being as visibly distinct as the moving bed to settled bed transition, which is clearly distinguishable, having no overlap.

The identification of a settling factor to quantify the intensity of the settling in the fluid can be used in the design of pipeline transfer processes, as a minimum bulk velocity can be calculated and avoided (with a safety factor appropriate for that application), in order to avoid unwanted sedimentation occurring during a pipe transfer operation. Even though the boundaries between all the different regimes are not perfectly distinguished, it would still be extremely useful to know that a particular pipeline operation fell close to one of these boundaries and as such there was a chance (risk) of either of the two settling regimes occurring in that pipeline (or likely both occurring at different longitudinal locations in a very long pipe).

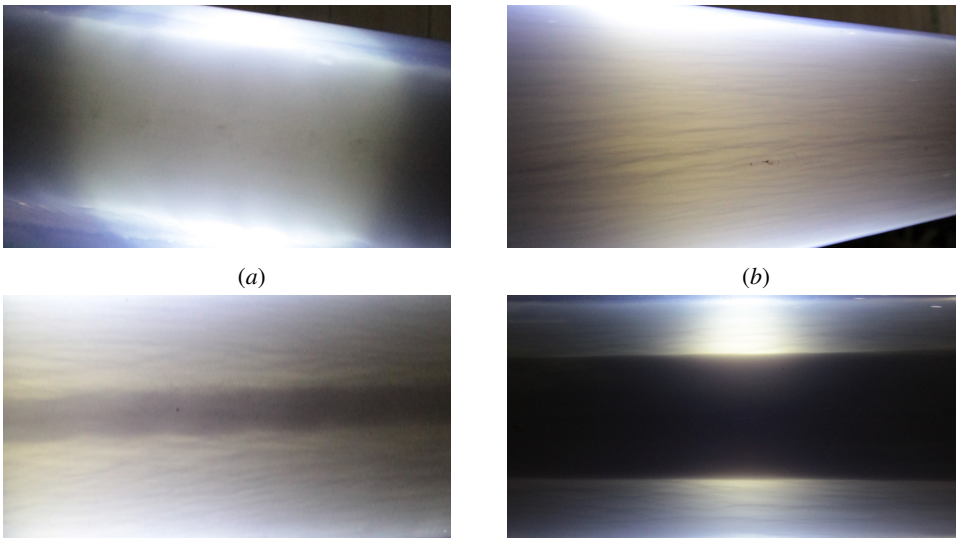

(*a*) (*b*)

(*c*) (*d*)

Figure 11: Images of settling regimes as viewed from underneath the STR D3i (or D4i) pipeline: (a) homogeneous suspension, (b) dynamic pathlines, (c) moving bed and (d) settled bed. The working fluid is B60 in these photographs, but the images are also representative of the other working fluids.

Settling regime	Settling factor
Homogeneous suspension	$\varsigma < 0.224$
(overlap region)	$(0.200 < \varsigma < 0.247)$
Dynamic pathlines	$0.224 < \varsigma < 0.356$
(overlap region)	$(0.346 < \varsigma < 0.366)$
Moving bed	$0.356 < \varsigma < 0.498$
Settled bed	$\varsigma > 0.498$

Table 6: Values of settling factor for each of the four settling regimes.

The critical deposition velocity is the velocity below which solid particles are unable to remain in motion and settle (Brown and Heywood, 1991). Using the above definition of the settling regimes this would be when a settled bed forms, thus $\varsigma = 0.498$ is the critical deposition settling factor, which would be used (along with the material properties) to calculate the critical deposition velocity. Similarly, a sedimentation velocity can be defined as the velocity at which sedimentation behaviour begins to occur (Doron et al., 1987). This corresponds to the dynamic pathlines regime in our framework and hence the sedimentation settling factor is $\varsigma = 0.224$, but could be as low as $\varsigma = 0.200$.

6. Practical application of Fresco and settling factor

Fresco and the settling factor (ς) can be utilised for the design and operation of flows through partially-filled pipes (and open channel flows more generally). In practical applications in many areas of industry and civil engineering, typically two key parameters are used to govern pipe transfers, these are the flow rate (Q) and the channel slope (S). These two parameters are used due to their practicality and simple measurability. Significant design requirements include the cost-effectiveness of the transfer as well as the status of sedimentation present in the pipeline. In areas such as sewage treatment and nuclear waste, it is required that the contents of the slurry remain suspended to avoid any settling and blockages of the conduit. However, dilution of the slurry through the addition of large volumes of water to ensure the safe transfer is undesirable due to the detrimental financial and environmental consequences. Hence an optimisation problem is presented where sediment must be transported in the most cost-effective manner possible. The research described in

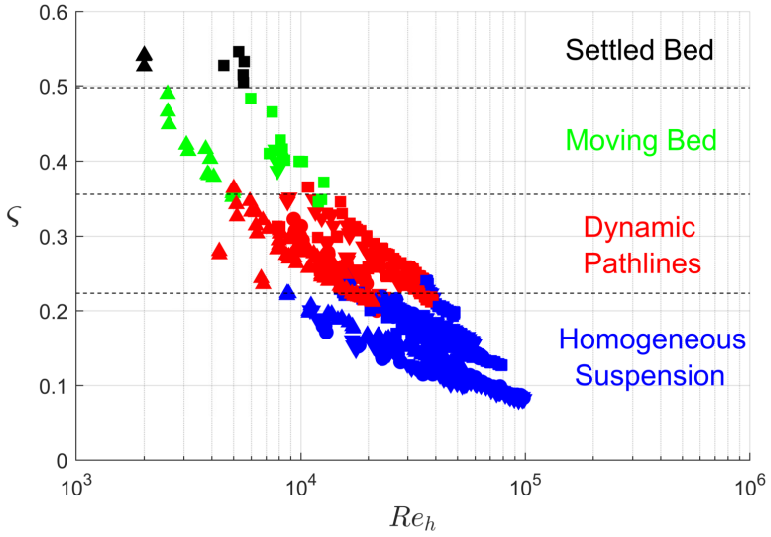

Figure 12: Settling Factor as a function of hydraulic Reynolds number for C40 (inverted triangles), C60 (circles), B40 (squares) and B60 (triangles). Data are coloured by the observed settling regimes of homogeneous suspension (blue), dynamic pathlines (red), moving bed (green) and settled bed (black). Dashed lines indicate approximate boundaries between different regimes.

this paper can assist with this problem by providing more knowledge on the underpinning transport fundamentals of these slurries.

As an example of how Fresco and settling factor (§4 and §5) can be utilised, we consider a typical design scenario involving the calculation of the minimum volumetric flow rate required to achieve a zero-sedimentation transfer on a partially filled pipeline with a known gradient. The settling factor and Fresco can be employed to determine a relationship between Q and ς. Combining equation 17 (Fresco) with equation 21 (settling factor) yields, equation 22,

$$\varsigma = \frac{\rho_p - \rho_f}{\rho} \frac{\nu_f}{d_p} \frac{4^{\frac{1}{9}} \nu(\theta)^{\frac{1}{9}}}{c g^{\frac{5}{9}} R_h(\theta)^{\frac{2}{3}} S^{\frac{1}{2}}}, \tag{22}$$

where the slurry kinematic viscosity (ν) and hydraulic radius (R_h) are both functions of θ. That R_h is a function of fill-angle is obvious and given by the geometric relationship of equation 4. Kinematic viscosity being a function of fill angle is perhaps less clear, but is a result of the non-Newtonian nature of the fluid. The viscosity in Fresco is that determined at a characteristic shear rate of the flow (as in Re_h), which we determine from the mean wall shear stress in the pipe (τ_w). The wall shear stress is related to the hydraulic radius through equation 12 and is therefore a function of θ. Getting from τ_w to ν is achieved through the rheology of the particular fluid (as in §3.3) or an appropriate rheological model.

Fresco can also be re-dimensionalised in an expression for Q, shown in equation 23,

$$Q = AU_b = A(\theta) \frac{c}{4^{\frac{1}{9}} \nu(\theta)^{\frac{1}{9}}} g^{\frac{5}{9}} R_h(\theta)^{\frac{2}{3}} S^{\frac{1}{2}}. \tag{23}$$

This presents a set of equations coupled by the fill angle (θ), which can be solved using numerical techniques.

To facilitate our example, an algorithm was written to solve equation 22 iteratively for the implicit θ at a given ς. Once θ is known, equation 23 is used to find the corresponding Q at this location. In this example, test material B40 is used on a pipeline D3i set at a 1.5% gradient. Figure 13 (a) shows the solution to equations 22 and 23 with the line coloured by the settling regimes it is passing through. As $d/D \to 0$, $Q \to 0$ and $\varsigma \to \infty$, however as $d/D \to 1$ a finite ς is observed at the upper limit of Q, the minimum ς occurs at $d/D \approx 0.8$ with the maximum Q occurring at $d/D \approx 0.9$. To achieve a homogeneous suspension the settling factor must be $\varsigma < 0.224$, hence a flow rate of $Q \gtrsim 8.0$ m^3/hr is required. Figure 13 (b) shows the solution for test material C60 on a pipeline D3i set at a 1% gradient, here a flow rate of $Q \gtrsim 3.0$ m^3/hr is required for a homogeneous suspension. It is worth noting that we have included our experimental data on figure 13 for reference, but for the

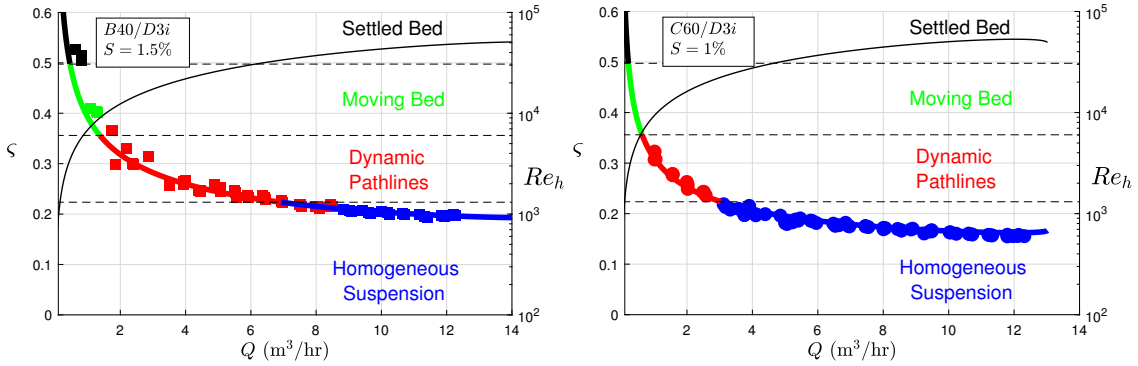

(a) (b)

Figure 13: Settling factor (coloured line, left hand axis) and Reynolds number (black line, right hand axis) as a function of flow rate for (a) B40, D3i and $S = 1.5\%$, experimental data shown by squares and (b) C60, D3i and $S = 1\%$, experimental data shown by circles.

	B40 on D3i at $S = 1.5\%$		C60 on D3i at $S = 1\%$	
Settling regime	Re_h	U_b (m/s)	Re_h	U_b (m/s)
Homogeneous suspension	> 33603	> 0.87	> 22397	> 0.61
(overlap region)	25317 – 46027	0.79 – 0.97	17108 – 30215	0.55 – 0.68
Dynamic pathlines	8991 – 33603	0.54 – 0.87	6388 – 22397	0.38 – 0.61
(overlap region)	8313 – 9747	0.53 – 0.56	5928 – 6898	0.37 – 0.39
Moving bed	3485 – 8991	0.39 – 0.54	2592 – 6388	0.27 – 0.38
Settled bed	< 3485	< 0.39	< 2592	< 0.27

Table 7: Values of Re_h, Q and U_b for their corresponding settling regimes.

purposes of this example application the experimental data is *completely unnecessary*. The hydraulic Reynolds number can also be calculated using Fresco and is plotted against the right hand vertical axis in figure 13. A summary of the flow conditions for each settling regime is shown in table 7. It may be advisable to add a safety factor on to these values to account for various scenario errors.

7. Summary and conclusion

Predicting the flow of slurries through partially filled conduits (or open channels) is highly relevant to many industries, such as nuclear, sewerage and mining. Two aspects which are of primary importance are the flow characteristics and the sedimentation characteristics. This work enables the prediction of both the flow and settling behaviour of slurries through correlations based on dimensional analysis, which have been shown to perform well in gravity-driven partially filled pipelines of non-colloidal suspensions. Experiments were conducted on two different cylindrical pipes (3-inch and 4-inch diameter) and data was collected for Reynolds numbers in the range of $2 \times 10^3 \leq Re \leq 1 \times 10^5$, Froude numbers in the range of $1.1 \leq Fr \leq 4.4$, and channel gradients of 0.5%, 1%, 1.5% and 5%. The experimental tests are supported by comprehensive characterisation of the working fluids through measurements of the particle size distribution, static settling velocities and shear rheology (utilising a specific protocol to avoid settling during the rheological measurement). Four different working fluids were used, two concentrations of each calcium carbonate and barium sulphate in water. Each was found to have a non-Newtonian shear thinning character (consistent with the literature), which was well represented by a power-law in the shear-rate range of interest.

In terms of flow, the Manning equation has long been used to predict the bulk velocity of open channel flows. In this work it was again shown to be a good tool for predicting the bulk velocity of water, however, a significant

error emerged when fluids with different density and viscosity values were used. It therefore cannot be used to accurately predict slurry flows (or multiphase and non-Newtonian flows more generally). A new correlation (Fresco) was developed which expresses the nexus between the hydraulic Reynolds number, Froude number and channel gradient through a single, constant, dimensionless coefficient (c). This correlation was shown to be significantly more accurate at predicting the bulk velocity than the original Manning equation, due largely to the inclusion of the physical properties of the test material. Unlike Manning's n coefficient, this c factor is non-dimensional and constant (within experimental uncertainty) across all working fluids tested and has an empirically-derived value of $c = 5.6$ (at least for hydraulically smooth pipes).

With regard to the transport of solids, four different settling regimes were observed across the range of experimental tests, ranging from no settling (homogeneous suspension) to a static bed being formed on the lower portion of the pipe wall. A non-dimensional settling factor was developed based on the competing factors of the density difference between the solid and liquid phases and the bulk flow of fluid down the pipe (which can be calculated using Fresco). This settling factor (ς) was shown to reliably predict the settling regime observed in the pipeline, with a value of ς being valid across the range of experiments (i.e. no adjustment to this value is required to account for hydraulic Reynolds number, Froude number, slope, working fluid, or pipe diameter). The settling factor combined with the flow correlation (Fresco) provide a powerful framework for predicting the likely settling regime observed for pipeline processes involving slurries, which is crucial to avoid failures (e.g. blockages) which can have serious consequences.

The development of correlations which have been shown to accurately predict the transport and settling behaviour of fluids representative of nuclear waste material, provides a way of underpinning the behaviour of multiphase flows typical to nuclear plant operations. This therefore allows for more refined transfer operations, increasing plant reliability and gaining further knowledge of the transport and sedimentation characteristics of the material. Although this research was conducted with the nuclear industry considered as the primary industrial application, the correlations have been developed in the most generic way possible in order to make them universally applicable to slurry flows in general.

Acknowledgments

This work was supported by the Centre for Innovative Nuclear Decommissioning (CINDe), which is led by the National Nuclear Laboratory (NNL), in partnership with Sellafield Ltd and a network of Universities that includes the University of Manchester, Lancaster University, the University of Liverpool and the University of Cumbria. The authors would like to thank the CINDe management team for their contribution to the completion of this work. The authors would also like to acknowledge the NNL Remote Engineering Team and the NNL Workington Process Team for their help and support with this work, as well as George McArthur at Sellafield Ltd. for his advice and support. CJC would like to acknowledge the funding for his PhD from the Engineering and Physical Sciences Research Council (EPSRC) in the form of an Industrial CASE award.

References

Adamson, D., 2011. Demonstration Of Mixing And Transferring Settling Cohesive Slurry Simulants In The AY-102 Tank. Tech. rep., Savannah River Site.

Akgiray, Ö., 2004. Simple formulae for velocity, depth of flow, and slope calculations in partially filled circular pipes. Environmental Engineering Science 21 (3), 371–385.

Akgiray, Ö., 2005. Explicit solutions of the Manning equation for partially filled circular pipes. Canadian Journal of Civil Engineering 32 (3), 490–499.

Arcement, G. J., Schneider, V. R., 1989. Guide for selecting Manning's roughness coefficients for natural channels and flood plains.

Attari, M., Hosseini, S. M., 2019. A simple innovative method for calibration of Manning's roughness coefficient in rivers using a similarity concept. Journal of Hydrology 575, 810–823.

Barnes, H. A., Hutton, J. F., Walters, K., 1989. An Introduction to Rheology. Vol. 3. Elsevier.

Barr, D. I. H., Das, M. M., Manning, 1986. Direct solutions for normal depth using the Manning equation. Proceedings of the Institution of Civil Engineers 81 (3), 315–333.

Bishop, R. R., 1978. Hydraulic characteristics of PVC pipe in sanitary sewers (a report of field measurements). Reports of Utah Water Research Laboratory 598.

Bishop, R. R., Jeppson, R. W., 1975. Hydraulic characteristics of PVC sewer pipe in sanitary sewers. Utah State University. Logan, Utah.

Blinco, P. H., Partheniades, E., 1971. Turbulence characteristics in free surface flows over smooth and rough boundaries. Journal of Hydraulic Research 9 (1), 43–71.

Brown, N. P., Heywood, N. I., 1991. Slurry Handling: Design of solid-liquid systems. Springer Science & Business Media.

Burger, J., Haldenwang, R., Alderman, N., 2010a. Experimental database for non-Newtonian flow in four channel shapes. Journal of Hydraulic Research 48 (3), 363–370.

Burger, J., Haldenwang, R., Alderman, N., 2010b. Friction factor-Reynolds number relationship for laminar flow of non-Newtonian fluids in open channels of different cross-sectional shapes. Chemical Engineering Science 65 (11), 3549–3556.

Camp, T. R., 1946. Design of sewers to facilitate flow. Sewage Works Journal 18 (1), 3–16.

Chatterjee, S., Sugilal, G., Prabhu, S. V., 2017. Flow transitions in a partially filled rotating inclined pipe with continuous flow. Experimental Thermal and Fluid Science 83, 47–56.

Cheng, N.-S., 1997. Effect of concentration on settling velocity of sediment particles. Journal of Hydraulic Engineering 123 (8), 728–731.

Chow, V. T., 1959. Open Channel Hydraulics. McGraw-Hill, New York, United States.

Christensen, B. A., 1984. Discussion of flow velocities in pipelines by Richard D. Pomeroy (August, 1983). Journal of Hydraulic Engineering 110 (10), 1510–1512.

Clausnitzer, B., Hager, W. H., 1997. Outflow characteristics from circular pipe. Journal of Hydraulic Engineering 123 (10), 914–917.

Coulson, J. M., Richardson, J. F., Backhurst, J. R., Harker, J. H., 1993. Motion of particles in a fluid. Chemical Engineering 2, 95–129.

Doron, P., Granica, D., Barnea, D., 1987. Slurry flow in horizontal pipesexperimental and modeling. International Journal of Multiphase Flow 13 (4), 535–547.

Dunnett, B., Ward, T., Roberts, R., Cheesewright, J., 2016. Physical properties of highly active liquor containing molybdate solids. In: Proceedings of the ATALANTE Conference on Nuclear Chemistry for Sustainable Fuel Cycles, Montpellier, France. pp. 5–10.

Durand, R., 1953. Basic Relationships of the Trnsportation of solids in Pipes-Experimental Research. Intern. Assoc. Hydr. Res., 5th Congr. Minneapolis, 1953.

Enfinger, K. L., Schutzbach, J. S., 2005. Scattergraph Principles and Practice: Camp's Varying Roughness Coefficient Applied to Regressive Methods. In: Pipelines 2005: Optimizing Pipeline Design, Operations, and Maintenance in Today's Economy. pp. 72–83.

Fitton, T. G., 2008. Non-Newtonian open channel flow: A simple method of estimation of laminar/turbulent transition and flow resistance. In: Paste. pp. 245–251.

Gioia, G., Bombardelli, F. A., 2001. Scaling and similarity in rough channel flows. Physical Review Letters 88 (1), 014501.

Haldenwang, R., 2003. Flow of non-Newtonian fluids in open channels. Ph.D. thesis, Cape Technikon.

Knight, D. W., Sterling, M., 2000. Boundary shear in circular pipes running partially full. Journal of Hydraulic Engineering 126 (4), 263–275.

Kökpınar, M. A., Göğüş, M., 2001. Critical flow velocity in slurry transporting horizontal pipelines. Journal of Hydraulic engineering 127 (9), 763–771.

Lashgari, I., Picano, F., Breugem, W. P., Brandt, L., 2016. Channel flow of rigid sphere suspensions: particle dynamics in the inertial regime. International Journal of Multiphase Flow 78, 12–24.

LaViolette, M., 2017. On the history, science, and technology included in the Moody diagram. Journal of Fluids Engineering 139 (3).

Lide, D. R., 2007. CRC Handbook of Chemistry and Physics, 88th Edition. CRC Press, Taylor & Francis, Boca Raton, FL 2007, pp. p. 4–150.

Manning, R., Griffith, J. P., Pigot, T. F., Vernon-Harcourt, L. F., 1890. On the flow of water in open channels and pipes. Transactions of the Institution of Civil Engineers of Ireland.

Mays, L. W., 1999. Hydraulic design handbook. McGraw-Hill Professional Publishing.

McArthur, G. A. H., Tinsley, T. P., McKendrick, D., 2005. Development of a liquid jet sludge re-suspension model (used on pulse jets or jet ballasts). In: AIChE Annual Meeting, Conference Proceedings.

Miskin, I., Elliott, L., Ingham, D. B., Hammond, P. S., 1996. Steady suspension flows into two-dimensional horizontal and inclined channels. International Journal of Multiphase Flow 22 (6), 1223–1246.

Nezu, I., Rodi, W., 1986. Open-channel flow measurements with a laser Doppler anemometer. Journal of Hydraulic Engineering 112 (5), 335–355.

Ng, H. C.-H., Cregan, H. L. F., Dodds, J. M., Poole, R. J., Dennis, D. J. C., 2018. Partially filled pipes: experiments in laminar and turbulent flow. Journal of Fluid Mechanics 848, 467–507.

Nguyen, Q. D., Akroyd, T., De Kee, D. C., Zhu, L., 2006. Yield stress measurements in suspensions: an inter-laboratory study. Korea-Australia Rheology Journal 18 (1), 15–24.

Paul, N., Biggs, S., Edmondson, M., Hunter, T. N., Hammond, R. B., 2013. Characterising highly active nuclear waste simulants. Chemical Engineering Research and Design 91 (4), 742–751.

Peker, S. M., Helvaci, S. S., 2011. Solid-liquid two phase flow. Elsevier.

Phillips, J. V., Tadayon, S., 2006. Selection of Manning's roughness coefficient for natural and constructed vegetated and non-vegetated channels, and vegetation maintenance plan guidelines for vegetated channels in Central Arizona. US Geological Survey.

Poloski, A. P., Bonebrake, M. L., Casella, A. M., Johnson, M. D., Toth, J. J., Adkins, H. E., Chun, J., Denslow, K. M., Luna, M., Tingey, J. M., 2009. Deposition velocities of non-Newtonian slurries in pipelines: complex simulant testing. Tech. rep., Pacific Northwest National Lab.(PNNL), Richland, WA (United States).

Poloski, A. P., Etchells, A. W., Chun, J., Adkins, H. E., Casella, A. M., Minette, M. J., Yokuda, S. T., 2010. A pipeline transport correlation for slurries with small but dense particles. The Canadian Journal of Chemical Engineering 88 (2), 182–189.

Pomeroy, R. D., 1983. Flow velocities in pipelines. Journal of Hydraulic Engineering 109 (8), 1108–1117.

Powell, R. W., 1960. History of Manning's formula. Journal of Geophysical Research 65 (4), 1310–1311.

Recknagle, K. P., 1999. Transport of Tank 241-SY-101 Waste Slurry: Effects of Dilution and Temperature on Critical Pipeline Velocity. Tech. rep., Pacific Northwest National Lab.

Rice, H. P., Fairweather, M., Hunter, T. N., Peakall, J., Biggs, S. R., 2017. The influence of relative fluid depth on initial bedform dynamics in closed, horizontal pipe flow. International Journal of Multiphase Flow 93, 1–16.

Rice, H. P., Fairweather, M., Peakall, J., Hunter, T. N., Mahmoud, B., Biggs, S. R., 2015. Constraints on the functional form of the critical deposition velocity in solid–liquid pipe flow at low solid volume fractions. Chemical Engineering Science 126, 759–770.

Rice, H. P., Pilgrim, J. L., Fairweather, M., Peakall, J., Harbottle, D., Hunter, T. N., 2020. Extending acoustic in-line pipe rheometry and friction factor modelling to low-Reynolds-number, non-Newtonian slurries. AIChE Journal, e16268.

Saatci, A., 1990. Velocity and depth of flow calculations in partially filled pipes. Journal of Environmental Engineering 116 (6), 1202–1208.

Souza Pinto, T., Moraes Junior, D., Slatter, P., et al., 2014. Modelling the critical velocity for heterogeneous flow of mineral slurries. International Journal of Multiphase Flow 65, 31–37.

Spedding, P. L., Chen, J. J. J., 1984. Holdup in two phase flow. International Journal of Multiphase Flow 10 (3), 307–339.

Swamee, P. K., 1995. Design of sediment-transporting pipeline. Journal of Hydraulic Engineering 121 (1), 72–76.

Swaminathan, T. N., Mukundakrishnan, K., Hu, H. H., 2006. Sedimentation of an ellipsoid inside an infinitely long tube at low and intermediate Reynolds numbers. Journal of Fluid Mechanics 551, 357–385.

Tominaga, A., Nezu, I., Ezaki, K., Nakagawa, H., 1989. Three-dimensional turbulent structure in straight open channel flows. Journal of Hydraulic Research 27 (1), 149–173.

Turian, R. M., Ma, T. W., Hsu, F. L. G., Sung, D. J., 1997. Characterization, settling, and rheology of concentrated fine particulate mineral slurries. Powder Technology 93 (3), 219–233.

Wang, Y., Lam, K. M., 2020. Clustering behaviour and settling velocity of bidisperse inertial particles in turbulent open channel flow. International Journal of Multiphase Flow, 103303.

Wasp, E. J., Kenny, J. P., Gandhi, R. L., 1977. Solid–liquid flow: slurry pipeline transportation.[Pumps, valves, mechanical equipment, economics]. Ser. Bulk Mater. Handl.;(United States) 1 (4).

Wasp, E. J., Slatter, P. T., 2004. Deposition velocities for small particles in large pipes. In: Proc. 12th International Conference on Transport & Sedimentation of Solid Particles, Prague, Czech Republic. pp. 20–24.

Wells, B. E., Kurath, D. E., Mahoney, L. A., Onishi, Y., Huckaby, J. L., Cooley, S. K., Burns, C. A., Buck, E. C., Tingey, J. M., Daniel, R. C., et al., 2011. Hanford waste physical and rheological properties: Data and gaps. Tech. rep., Pacific Northwest National Lab.(PNNL), Richland, WA (United States).

Wilcox, E. R., 1924. A comparative test of the flow of water in 8-inch concrete and vitrified clay sewer pipe. Washington State University.

Yen, B. C., 1992. Dimensionally homogeneous Manning's formula. Journal of Hydraulic Engineering 118 (9), 1326–1332.

Yoon, J.-I., Sung, J., Ho Lee, M., 2012. Velocity profiles and friction coefficients in circular open channels. Journal of Hydraulic Research 50 (3), 304–311.

Yu, G., Lim, S.-Y., 2003. Modified Manning formula for flow in alluvial channels with sand-beds. Journal of Hydraulic Research 41 (6), 597–608.

Yu, Z., Phan-Thien, N., Tanner, R. I., 2004. Dynamic simulation of sphere motion in a vertical tube. Journal of Fluid Mechanics 518, 61–93.

Zaghloul, N. A., 1998. Flow simulation in circular pipes with variable roughness using SWMM-EXTRAN model. Journal of Hydraulic Engineering 124 (1), 73–76.